Pharm Res (2020) 37:93
https://doi.org/10.1007/s11095-020-02807-x

RESEARCH PAPER

Drug Permeability Profiling Using the Novel Permeapad® 96-Well Plate

Ann-Christin Jacobsen [1] • Sune Nielsen [1] • Martin Brandl [1] • Annette Bauer-Brandl [1]

Received: 24 December 2019 / Accepted: 23 March 2020

ABSTRACT

Purpose Here, first experiences with a prototype tool for high throughput (passive) permeability profiling, a 96-well plate comprising the Permeapad® membrane, are reported. The permeabilities of a set of drugs were determined and compared to published measures of oral absorption, such as human fraction absorbed (F_a) and *in vitro* permeability values obtained using other tools.

Methods The tool consists of a 96-well bottom and screen plate with the artificial, phospholipid-based barrier (Permeapad®) mounted between the plates' lower and upper compartments. The permeability of 14 model compounds including high- and low-absorption drugs, cationic, anionic, zwitterionic and neutral molecules, was determined by quantifying the compounds' transport over time, deriving the steady-state flux from the linear part of the cumulative curves and calculating the apparent permeability (P_{app}). The membrane structure was investigated in a high-resolution digital light microscope.

Results The Permeapad® 96-well plate was found suited to distinguish high and low absorption drugs and yielded a hyperbolic correlation to F_a. The P_{app} values obtained were congruent with those determined with in-house prepared Permeapad® in the Franz cell set-up. Furthermore, good to excellent correlations were seen with Caco-2 permeability ($R^2 = 0.70$) and PAMPA permeability ($R^2 = 0.89$). Microscopic investigation of the Permeapad® barrier revealed the formation of phospholipid vesicles and myelin figures in aqueous environment.

Conclusion The Permeapad® 96-well plate permeation set-up is a promising new tool for rapid and reproducible passive permeability profiling.

KEY WORDS 96-well plate · artificial barrier · high throughput · intestinal absorption · microplate · permeability

ABBREVIATIONS

F_a	Fraction absorbed in humans
HPLC	High-performance liquid chromatography
PAMPA	Parallel artificial membrane permeability assay
P_{app}	Apparent permeability
PBS	Phosphate buffered saline
PVDF	Polyvinylidene fluoride
PVPA	Phospholipid vesicle-based permeation assay
TFA	Trifluoroacetic acid
TPSA	Total polar surface area
UHPLC-UV	Ultra-high-performance liquid chromatography with ultraviolet detection
UWL	Unstirred water layer

INTRODUCTION

Permeability is a key characteristic of drug molecules determining their fate after oral administration towards uptake and bioavailability. Experimentally, the permeability properties of drug molecules are determined using a wide variety of methods that range from complex *in situ* intestinal perfusion set-ups (e.g. closed-loop Doluisio model) to less complex *in vitro* cell-based permeation set-ups (e.g. Caco-2 cell-line) and to simple, artificial, cell-free permeation set-ups (e.g. parallel artificial

Electronic supplementary material The online version of this article (https://doi.org/10.1007/s11095-020-02807-x) contains supplementary material, which is available to authorized users.

✉ Annette Bauer-Brandl
annette.bauer@sdu.dk

[1] Drug Transport & Delivery Group, Department of Physics, Chemistry & Pharmacy, University of Southern Denmark, 5230 Odense, Denmark

Published online: 11 May 2020

membrane permeability assay; PAMPA). In contrast to tissue and cell-based permeation models, cell-free permeation models can only predict passive drug transport. Still, it can be advantageous to use these non-cellular permeation models due to their cost and time efficiency. Especially, in drug discovery and early development phases, where a large number of drug candidates require permeability characterization, cost and time efficiency is crucial. Besides the practical aspects of cell-free permeation tools, non-saturable passive transport is in the majority of cases regarded as the primary permeation route while active transport primarily plays a role for low permeability drugs and mainly at biological barriers other than the intestinal barrier (1). Recently, the use of cell-free permeation models for drug permeability profiling has been reviewed (2).

The most prominent cell-free permeation tool is the PAMPA model that was first described in 1998 by Kansy and co-workers (3) and since numerous modifications have been suggested (4,5). Common for all PAMPA barriers is that they are constructed of a filter (e.g. polyvinylidene fluoride; PVDF), soaked with phospholipids (e.g. egg phosphatidylcholine) dissolved in an organic solvent (e.g. n-dodecane) (2). Another approach is the phospholipid vesicle-based permeation assay (PVPA) that was first described in 2006 by Flaten and co-workers (6). The PVPA barrier is also constructed of a filter (mixed cellulose-ester) but the PVPA does not contain an organic solvent. Instead in this model, liposomes prepared by film-hydration and filter extrusion are deposited on the filter support by centrifugation. In 2015 di Cagno and co-workers introduced the Permeapad® model (7). This biomimetic, cell-free permeation barrier is the focus of this study. In contrast to the PAMPA and the PVPA barrier, the Permeapad® barrier is not based on a filter support. Instead, it is constructed as a sandwich of two cellulose-hydrate membranes enclosing a layer of dry phospholipids between them. Other than the PAMPA and the PVPA barrier, the Permeapad® barrier has a good storage stability. After preparation, it can be stored at room temperature in dry and light protected conditions at least for one year (7).

In its dry form, Permeapad® appears as a translucent membrane. However, in contact with aqueous media, the dry phospholipids enclosed between the support-sheets swell and give the barrier a milky appearance. Microscopic structures arising from phospholipids in contact with aqueous media are well described in literature (8). However, the microscopic structure of the Permeapad® barrier after swelling has not been studied. Regarding its functionality, the Permeapad® barrier was found to be promising for permeation testing of small molecules (7,9). Due to its high robustness against extreme pH values and aggressive additives (7,10), the Permeapad® model has also been employed in early formulation development. In more detail, the influence of polymer-based (11), (phospho)lipid-based (12–15) and surfactant-based drug formulations (16,17) on drug permeation has been investigated.

In previous studies, the Permeapad® barrier was prepared manually in-house and mounted in Franz or side-by-side diffusion cells to conduct permeation experiments. However, in drug discovery as well as early drug development, such set-ups appear inappropriate due to their limited throughput. Here, a new Permeapad® format, the Permeapad® Plate, is being tested for the first time. The Permeapad® Plate is a 96-well microtiter plate system that consists of a bottom plate and a screen plate to which the Permeapad® barrier is mounted in a way that it separates the plates' lower and upper compartments. For this novel format, the Permeapad® barrier was produced in industrial scale. Compared to the Franz cell or side-by-side set-up, permeation experiments in a 96-well format can significantly increase the throughput. Thereby, the Permeapad® model may become more useful for early permeability profiling and/or early formulation development.

The aim of this study was to evaluate a 96-well permeation system comprising the Permeapad® membrane for permeability profiling. To this end, a suitable methodology for permeation experiments was established by comparing the outcome of permeation experiments using different orientations of donor and acceptor in stirred or unstirred conditions. The permeability of selected model compounds including high and low absorption drugs was determined using the Permeapad® 96-well plate by following the compounds' transport across the barrier over time. For a detailed evaluation, the obtained permeabilities were then compared to published data on the fraction absorbed in humans and permeabilities determined using alternative methods (from literature). The alternative methods were: 1) the in-house prepared Permeapad® in Franz cells, 2) the Caco-2 model and 3) the PAMPA model. The Permeapad® 96-well plate and the in-house prepared Permeapad® were compared to investigate if these models yield comparable results despite the different preparation methods and shape/dimensions of the permeation device. Even though only passive drug transport can be illustrated, the Permeapad® 96-well plate was compared to the Caco-2 model because the Caco-2 model is currently considered as the 'gold-standard' for permeability profiling. Finally, the Permeapad® 96-well plate was compared to the PAMPA model because this model is the most commonly used method for passive permeability profiling today. An additional aim of this study was to investigate the microscopic structure of the Permeapad® barrier by light microscopy to gain a better insight into the functionality of the membrane.

MATERIALS AND METHODS

Chemicals

Fourteen structurally diverse compounds were selected for permeability profiling. Figure 1 shows the molecular structures and Table I gives calculated physicochemical properties of the compounds to illustrate the diversity of properties. Acyclovir, antipyrine, calcein, caffeine, carbamazepine, enalapril maleate, lucifer yellow, metoprolol tartrate, nadolol, naproxen, norfloxacin, sulpiride and terbutaline hemisulfate were purchased from Sigma-Aldrich® Denmark ApS (Brøndby, Denmark) and micronized hydrocortisone was purchased from Caesar & Lorentz GmbH (Hilden, Germany).

For the preparation of 29 mM phosphate buffered saline (PBS), sodium chloride was purchased from VWR™ International A/S (Søborg, Denmark), sodium dihydrogen phosphate monohydrate was purchased from Sigma-Aldrich® Denmark ApS (Brøndby, Denmark) and sodium hydroxide was purchased from Merck A/S (Hellerup, Denmark). All salts used for buffer preparation were of analytical grade.

Methanol (HPLC-grade) and trifluoroacetic acid (TFA; HPLC-grade) that were used for quantitative analysis were purchased from VWR™ International A/S (Søborg, Denmark).

Highly purified water was prepared using Milli-Q® reference A+ water purification system (Merck KGaA, Darmstadt, Germany) and was the only water quality used for permeability profiling and quantitative analysis.

Microscopic Evaluation of the Morphology of the Lipid Layer upon Swelling

Permeapad® barrier was provided by InnoMe GmbH (Espelkamp, Germany). A 1 cm^2 piece of membrane was placed on a microscope slide and wetted with water. After 10 min of incubation, the wetted barrier was covered with a cover glass. Microscopic images of the membrane structure were taken with a KEYENCE VHX-2000 digital light microscope connected to a VH-Z500R high-resolution zoom lens with a magnification of 500x to 5000x over a period of 1 h. The size of vesicular structures was estimated using ImageJ software.

Permeability Profiling

Preparation of Model Compound Solutions

1 mM solutions of the model compounds were prepared in PBS pH 6.5 ± 0.05 (255 ± 5 mOsm/kg). To aid the dissolution process, the model compounds were sonicated for approximately 30 min and stirred overnight under light protection when necessary. In case of the poorly soluble compounds, carbamazepine and hydrocortisone, 0.1 mM solutions were prepared. In case of the highly soluble marker calcein, a 5 mM solution was prepared.

Permeapad® Plate Design

Prototypes of Permeapad® Plate were provided by InnoMe GmbH (Espelkamp, Germany). The Permeapad® Plate is a two-compartment 96-well microtiter plate consisting of a bottom plate, a screen plate and a lid. In this device, the Permeapad® barrier is mounted to the bottom of the screen plate's wells with adhesive. Figure 2 shows details of the design of the Permeapad® Plate. The wells of the bottom plate have an unconventional shape with a maximum capacity of 400 µL (see Fig. 2a). In contrast, the wells of the screen plate have a round shape with a tilted bottom and with a maximum capacity of 200 µL (see Fig. 2b and c). By tilting the bottom, air-bubbles under the membrane are avoided and the permeation area increased. Additionally, the screen plate is equipped with a sampling port (located next to the opening of the upper well) that enables sampling from the bottom wells without disassembling the set-up. The available area for permeation is 0.15 cm^2.

Permeability Profiling – Influence of Orientation and Stirring

Due to the peculiar design of the Permeapad® Plate, it was investigated if using the bottom or screen plate as donor or acceptor compartment influenced the result of the permeation experiment. As examples, 1 mM antipyrine and 1 mM enalapril were used as donor solutions. Table II gives an overview of the tested orientations.

To conduct the permeation experiment, the donor solution and the acceptor media (29 mM PBS pH 7.4, 255 ± 5 mOsm/kg) were filled into the respective wells. Additionally, 5 × 2 mm magnetic stir bars were added to the bottom wells. After sealing the screen plate with pre-perforated, adhesive sealing foil (x-Pierce., Excel Scientific, Inc.) to minimize evaporation, the set-up was incubated at room temperature under stirring (500 rpm) using a 96-well plate magnetic stirrer (2mag AG, Munich, Germany). Samples (120 µL) were taken every 30 min from the respective acceptor compartment for 4 h and replaced with fresh PBS. The samples were analysed by UHPLC-UV (see section 2.3.5) and the data was treated as described in section 2.3.7.

Permeability Profiling of Model Compounds

For permeability profiling of all model compounds, the bottom-to-top orientation was used. In brief, 400 µL model compound solution was transferred to the bottom wells alongside a magnetic stir bar. The screen plate was placed on top

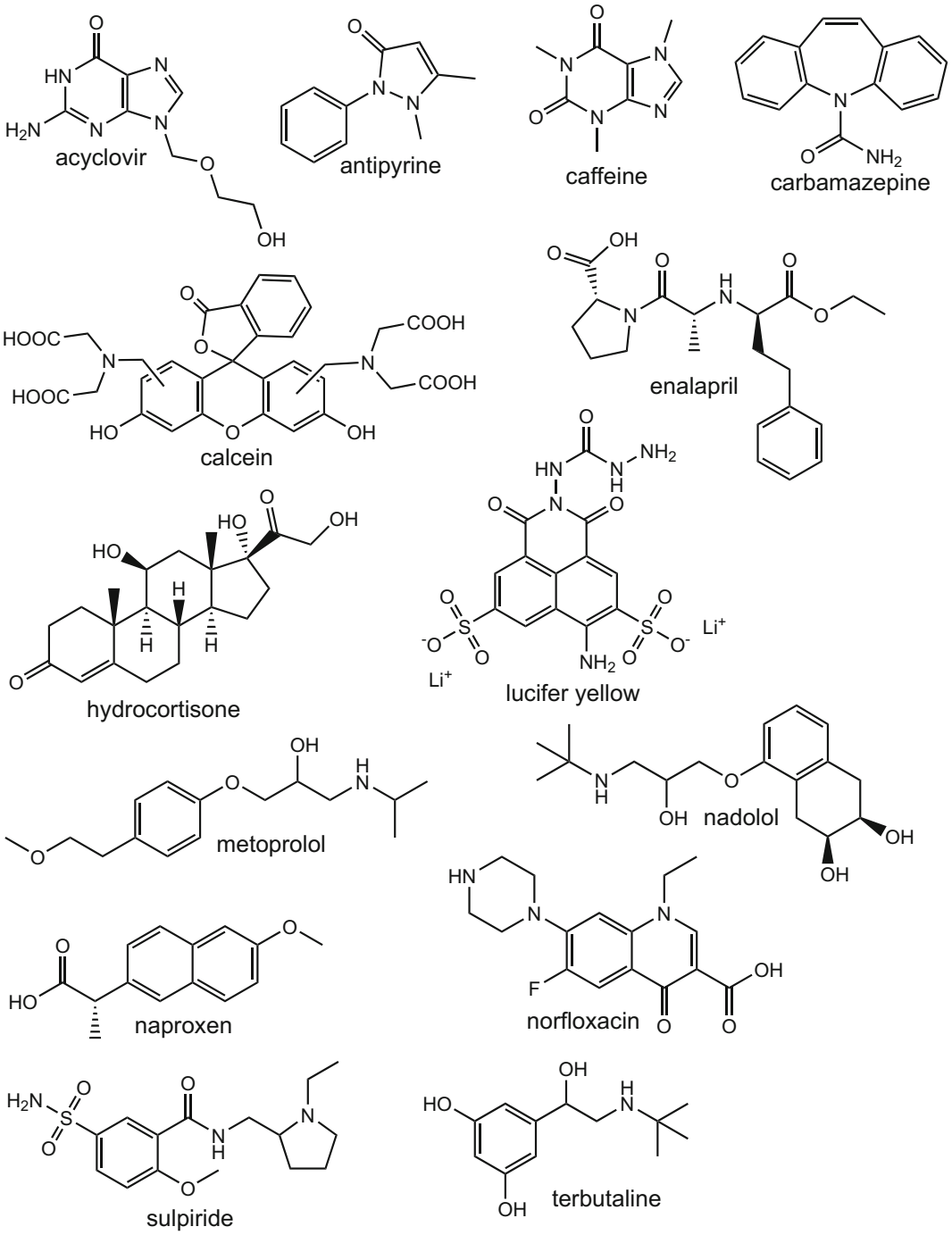

Fig. 1 Molecular structures of the model compounds.

and 200 µL PBS pH 7.4 was added. After sealing with adhesive sealing foil, the plate was incubated at room temperature under stirring (500 rpm) for 4 h. Every 30 min, 120 µL sample was taken from the top wells and replaced with fresh PBS. All samples were analysed by UHPLC-UV (see section 2.3.5) except for samples containing calcein and lucifer yellow, which were analysed using fluorescence spectroscopy (see section 2.3.6.). For all compounds, data was treated as described in section 2.3.7.

Quantification by UHPLC-UV

Ultra-high-performance liquid chromatography with ultraviolet detection (UHPLC-UV) was used for quantitative analysis of permeation samples due to extractables from the adhesive, which absorb UV-light in the range of 200–290 nm with an absorbance maximum at 250 nm (see supplementary material). As most of the model compounds have an absorbance maximum in this wavelength range and do not absorb

Table I Calculated Physicochemical Properties of the Model Compounds

Compound	Calculated properties[a]					
	molar mass (g/mol)	log P	pKa (s)	TPSA (Å^2)	Predominant charge at pH 6.5	Solubility at pH 6.5 (mg/mL)
Acyclovir	225.21	−1.03	3.02 11.98	115	0	9.10
Antipyrine	188.23	1.22	0.49	24	0	4.91
Caffeine	194.19	−0.07	−1.16	58	0	70.9
Calcein	622.53	−4.09	1.51 7.45	232	–	623
Carbamazepine	236.27	2.77	15.96	46	0	0.04
Enalapril	376.45	0.59	3.67 5.2	96	–	2.70
Hydrocortisone	362.47	1.28	12.59	95	0	0.41
Lucifer Yellow	442.3	−4.44	−2.78 3.03	233	±	>15[b]
Metoprolol	267.37	1.76	9.67 14.09	51	+	538
Nadolol	309.41	0.87	9.76 13.59	82	+	505
Naproxen	230.26	2.99	4.19	47	–	16.9
Norfloxacin	319.34	−0.97	5.58 8.77	73	±	2.94
Sulpiride	341.43	0.22	10.24 8.39	102	+	259
Terbutaline	225.29	0.44	8.86 9.76	73	+	3109

[a] obtained from chemicalize.com developed by ChemAxon (Budapest, Hungary) [b] Lucifer Yellow solubility could not be calculated, solubility was taken from (18)

(enough) UV-light above 290 nm, separation was required prior to UV analysis. It is worth mentioning that the adhesive used in routine production is different from the one used in the prototypes tested here according to the manufacturer.

UHPLC-UV analysis was conducted on a Thermo Fisher UltiMate 3000 UHPLC system that was connected to a diode array detector and equipped with a reversed phase Kinetex® EVO C18 LC-column (150 × 2.1 mm; particle size 1.7 µm; pore size 100 Å, Phenomenex®). Table III shows an overview of UHPLC conditions used for the analysis of the model drugs. The mobile phase consisted of methanol and 0.1% trifluoroacetic acid in purified water, the flow rate was 0.3 ml/min and the column oven was set to 50°C. Samples containing hydrocortisone were analysed at a flow rate of

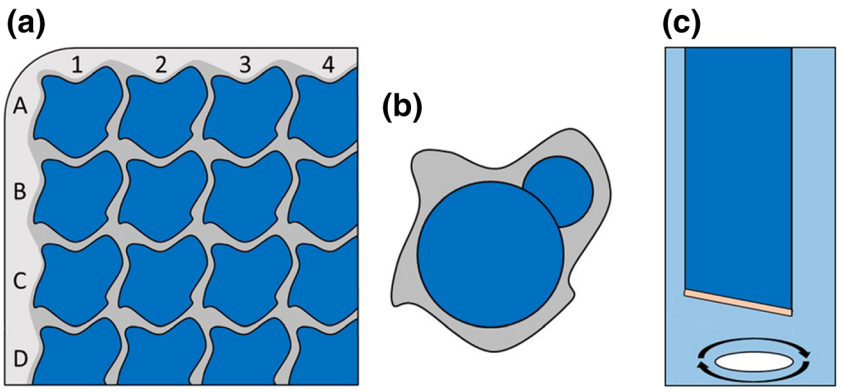

Fig. 2 Details of the design of the Permeapad® Plate. (**a**) View on the bottom plate from above, (**b**) View on the top well from above including the well itself (large circle) and the sampling port (small circle), and (**c**) Side view of the combined wells including the top-well (dark blue), the bottom-well (light blue), the Permeapad® barrier (orange) and an optional magnetic stir bar (white).

Table II Overview of Alternative Orientations for Permeation Experiments

Orientation	Donor volume	Acceptor volume	Sampling
Bottom-to-top	400 μL	200 μL	120 μL from top wells
Top-to-bottom	200 μL	400 μL	120 μL from the bottom wells through the sampling port

0.37 ml/min and a column oven temperature of 60°C. The injection volume was 5 μL. The samples were injected undiluted.

Calibration curves were prepared by dilution from stock solutions of the respective compound in PBS pH 7.4. The stock solutions that had a concentration well below the aqueous solubility of the compound were prepared like the donor solutions (see section 2.3.1). The range of the calibration curves is given in Table III.

Quantification of Markers by Fluorescence Spectroscopy

Samples containing calcein or lucifer yellow were analysed using a BMG FLUOstar® Omega microplate reader. For both compounds, the excitation and emission wavelengths were 485–12 and 520 nm, respectively. For calcein and lucifer yellow quantification, standards with concentrations of 0.1–4 μg/mL and 0.2–20 μg/mL, respectively, were prepared.

Data Analysis

To determine the apparent permeability (P_{app}) of the model compounds, the cumulative amount of compound permeated across the Permeapad® barrier (dQ) was normalized by the surface area (A; 0.15 cm^2) and plotted against time (dt). The linear part of this graph represents the compounds' flux ($\mathcal{J}$):

$$\mathcal{J} = \frac{dQ}{A \cdot dt}$$

Steady state was typically reached after 30 min. To calculate P_{app}, the flux was normalized by the concentration of the model compound solution (C_0):

$$P_{app} = \frac{\mathcal{J}}{C_0}$$

The permeation experiments were carried out with 3–6 replicates. The P_{app} of a model compound is expressed as the mean ± SD of the individual replicates' P_{app}.

RESULTS AND DISCUSSION

Microscopic Evaluation of the Morphology of the Lipid Layer upon Swelling

Figure 3 shows microscopic images of the wetted Permeapad® barrier at different magnifications. Here, myelin-like structures and vesicles typical for phospholipids were recognized. These structures had multiple lamellae. The multiple lamellae are best seen at the highest magnification (Fig. 3c). Using ImageJ software, the mean vesicular size was estimated to be 27.7 ± 9.5 μm. For the image-based size analysis Fig. 3a was used. Here, 44 vesicles were recognized and used for size-estimation.

The structures seen on Fig. 3 were not static during the microscopic evaluation. The movement of vesicles and bilayer structures is, however, expected as the artificial membrane does not contain any constituents that may anchor vesicles to

Table III Conditions for UHPLC-UV Analyses

Compound	0.1% TFA in water (%)	Methanol (%)	Detection wavelength (nm)	Retention time (min)	Concentration range of calibration (μg/mL)
Acyclovir	95	5	253	1.55	0.2–17
Antipyrine	60	40	242	1.63	0.3–20
Caffeine	55	45	274	1.41	0.2–150
Carbamazepine	45	55	300	1.98	0.1–23
Enalapril	65	35	206	3.45	0.3–60
Hydrocortisone	65	35	248	4.4	0.1–110
Metoprolol	55	45	274	3.1	0.5–50
Nadolol	70	30	202	1.98	0.2–20
Naproxen	50	50	232	3.95	0.3–26
Norfloxacin	65	35	286	1.54	0.1–20
Sulpiride	85	15	212	1.77	0.1–40
Terbutaline	85	15	206	1.61	0.2–30

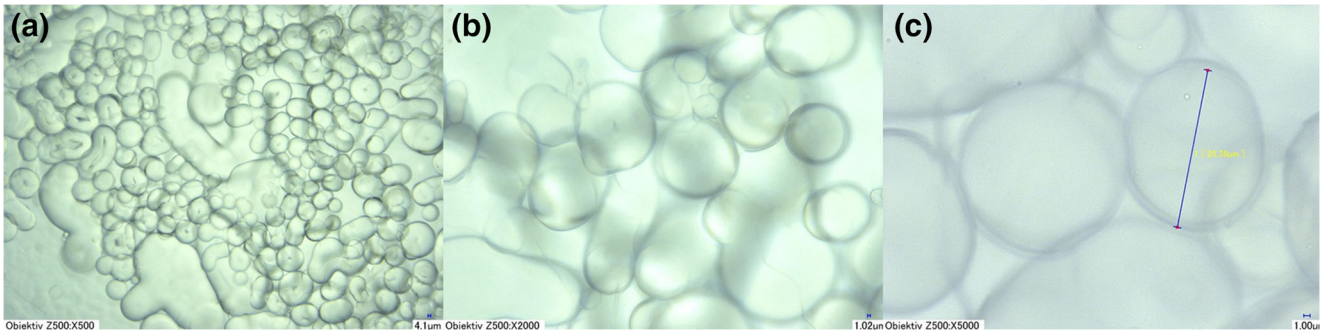

Fig. 3 Microscopic images of the wetted Permeapad® barrier at different magnifications: (**a**) ×500, (**b**) ×2000 and (**c**) ×5000.

each other or the support sheet. In wetted conditions, the Permeapad® barrier can thus be considered as a vesicular phospholipid gel (19,20) that is constrained within two cellulose-based support sheets. Of course, the flexibility of the Permeapad® microstructure contrasts the relative rigidity of the Caco-2 cell monolayer, where cells are connected by tight junctions.

The microscopic images of the Permeapad® barrier that are presented here are especially interesting because it previously has been difficult to describe the microscopic structure of other cell-free, artificial permeation barriers. For example, the microscopic structure of the PAMPA model is still unclear. Due to the presence of organic solvent, the PAMPA membrane possibly has a non-bilayer structure (21). In contrast to the PAMPA model, the microscopic structure of the PVPA model has been described in literature in more detail (22). In the PVPA model, liposomes are deposited on a filter support to form the permeation barrier. There may be similarities between the microscopic structure of the PVPA model and Permeapad® because both models mainly consist of phospholipids. However, the phospholipid vesicles in the PVPA model are more uniform in size because they are prepared according to a protocol beforehand whereas the vesicles in the Permeapad® model form spontaneously upon wetting between the cellulose-sheets. Furthermore, the phospholipid vesicles in the PVPA model are likely more static compared to the Permeapad® model because they are deposited in the porous filter support by centrifugation.

Permeability Profiling

Cell-free, artificial permeation methods are commonly considered as cost and time effective alternatives to tissue and cell-based *in vitro* permeation methods. In literature, various cell-free permeation barriers have been described as for example PAMPA, PVPA and Permeapad® (2). In this study, a novel 96-well plate for permeability profiling was evaluated. This study's main aims were to 1) establish a suitable methodology for permeation profiling, 2) compare permeation results obtained with the Permeapad® 96-well plate with those obtained with in-house prepared Permeapad® (in Franz cell format) and 3) characterize the ability of the Permeapad® 96-well plate to predict permeation properties. The Permeapad® 96-well plate was compared to the in-house prepared Permeapad® primarily to investigate if the results are comparable even though the plate contains an industrial version of the barrier and has a very different shape and dimensions than a Franz cell. Finally, the novel model's ability to predict permeation properties was characterized by comparing the apparent permeability coefficients (P_{app}) of 14 model compounds to literature values of the fraction absorbed in humans (F_a), Caco-2 P_{app} values and PAMPA P_{app} values.

Steady State Transport and Choice of Sampling Time

Two typical permeation curves, i.e. the cumulative amount of antipyrine and terbutaline permeated per area over time, are shown in Fig. 4. After an initial lag-time of typically 30 min, a clear linear relationship between the cumulative amount of compound permeated and time was observed when using the Permeapad® 96-well plate (i.e. steady state conditions). From this linear part of the graph, the P_{app} value of the model compounds was derived. For all tested compounds steady-state conditions were achieved after 30 min and maintained during the whole experiment (data not shown). In essence this means that to further increase throughput, P_{app} could reliably be derived from only two measurements after the short lag-time (approximately 30 min). On the other hand, multiple time points may be useful to ensure that steady-state conditions still apply. For high permeability compounds, the top-to bottom orientation (i.e. where the acceptor volume is larger than the donor volume) may thus be preferable (different orientations are discussed in the next section). This is worth mentioning because many *in vitro* permeation assays rely on one time-point only, not taking into account possible lag-times.

Influence of Orientation and Stirring

To identify a useful methodology for permeability profiling using the Permeapad® 96-well plate, different orientations in stirred and unstirred conditions were tested using the highly permeable compound antipyrine and the moderately

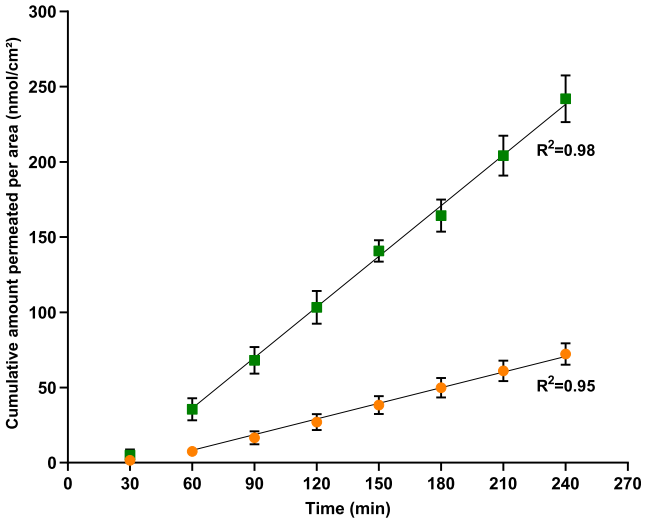

Fig. 4 Examples of typical permeation curves. The cumulative amount antipyrine (green squares) and terbutaline (orange circles) permeated across the Permeapad® barrier per area over time. Permeation curves are shown as the mean ± SD, $n = 6$.

permeable compound enalapril as examples. The results are summarized in Fig. 5. In more detail, Fig. 5 shows the P_{app} of antipyrine and enalapril when using either the bottom or the top plate as donor compartment (i.e. bottom-to-top or top-to-bottom orientation) with and without stirring. Stirring was always conducted in the bottom plate. Hence, in the bottom-to-top orientation the donor was stirred and in the top-to-bottom orientation the acceptor was stirred.

When introducing a new method, it is useful to investigate how different choices in the experimental set-up can affect the experiment's results. In the case of the Permeapad® 96-well plate, the peculiar shape of the bottom plate (Fig. 1a) may influence the hydrodynamics and thereby the thickness of the adherent unstirred water layer (UWL). The UWL has been recognized as a considerable permeation barrier for lipophilic/highly permeable drug compounds (23). Hence, even though Permeapad® is a symmetrical membrane, differences in the thickness of the UWL in either orientation may influence the permeation results. The thickness of the adherent UWL can be reduced by agitation/stirring (23,24). Therefore, these experiments were conducted under stirred or unstirred conditions.

In agreement with previous findings that showed that the permeability of less permeable compounds is not affected by the thickness of the UWL (23), neither the orientation nor the stirring conditions significantly affected the P_{app} of the moderately permeable compound enalapril in the Permeapad® 96-well plate (in all cases $p > 0.05$). Still, a small decrease in enalapril P_{app} was seen in unstirred conditions. Also, in agreement with previous findings, the P_{app} of the highly permeable compound antipyrine was significantly decreased when using the bottom-to-top orientation under unstirred conditions ($p < 0.05$). In contrast, when using the top-to-bottom orientation antipyrine's P_{app} was decreased but the difference between stirred or unstirred conditions was not significant ($p > 0.05$). These results indicate that especially when using the bottom-to-top orientation, it is important to include stirring/agitation. Otherwise, the permeability of lipophilic/highly permeable compounds can be underestimated. Possibly, the unconventional shape of the bottom-plate is the reason for why the effect of stirring on antipyrine's P_{app} is more pronounced in the bottom-to-top orientation. The unconventional shape may lead to a thicker UWL as compared to the conventional

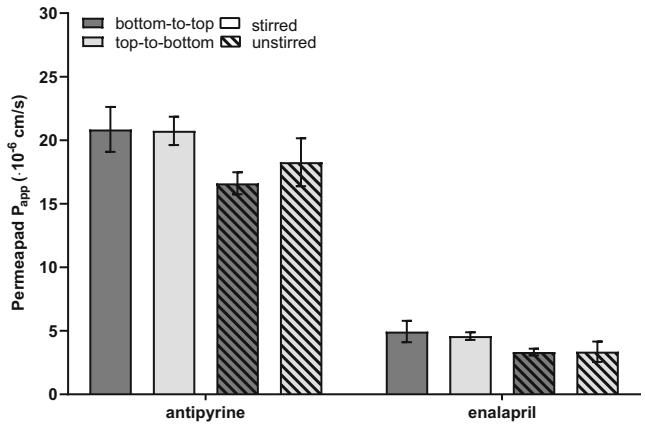

Fig. 5 The apparent permeability (P_{app}) of antipyrine ($n = 4$) and enalapril ($n = 3$) when using different orientations of the Permeapad® 96-well plate for permeation experiments with and without stirring. Dark grey and light grey columns indicate bottom-to-top and top-to-bottom orientations, respectively. Open and striped columns indicate stirred and unstirred conditions, respectively.

round shape of the top plate. Another reason may be differences in UWL when stirring donor and acceptor, respectively. With the current set-up stirring in both compartments is not possible. For further permeation experiments the bottom-to-top orientation was used due to ease of sampling.

Permeability Profiling of Model Compounds

The P_{app} values of the 14 model compounds determined using the Permeapad® 96-well plate are shown in Table IV. For comparison, Table IV also gives literature values for the fraction absorbed in humans and P_{app} values from the in-house prepared Permeapad®, the PAMPA model and the Caco-2 model. Generally, the permeation experiments using the Permeapad® 96-well plate were highly reproducible with typical standard deviations (SD) of 5–10%. In more detail, in 9 out of 14 experiments the SD was between 5 and 10%. The SD of the remaining 5 experiments was between 10 and 20%.

The in-house prepared Permeapad® barrier was originally described by di Cagno *et al.* in 2015 (7). In their study, the Permeapad® barrier was mounted in a Franz cell and the permeation experiments were carried out using PBS pH 7.4 in both donor and acceptor compartment. The two Permeapad® models differ thus not only with regard to the membrane preparation method but also with regard to the liquid volumes, shape of the permeation device and the pH conditions. Despite these differences, the P_{app} values from the Permeapad® 96-well plate generally were in acceptable agreement with P_{app} values from the in-house prepared Permeapad®. As can be seen in Table IV, among the compounds tested in both Permeapad® models, caffeine had the highest P_{app} value in both Permeapad® models. The P_{app} value of caffeine was $29.3 \pm 2.51 \times 10^{-6}$ cm/s in this study and $20.4 \pm 3.2 \times 10^{-6}$ cm/s in the previous study. In both models, hydrocortisone, a neutral compound, had the second highest P_{app} value. Here, the P_{app} value was the same in the two models with 12.3 ± 0.52 and $12.7 \pm 1.5 \times 10^{-6}$ cm/s. Also, in both models, calcein, a zero-permeability marker, had the lowest P_{app} value. The P_{app} value of calcein was $0.43 \pm 0.04 \times 10^{-6}$ cm/s in this study and $1.2 \pm 0.1 \times 10^{-6}$ cm/s in the previous study. The second lowest P_{app} was in both cases measured for nadolol.

In summary, the P_{app} ranking of compounds was similar in the two Permeapad® models except for metoprolol, and acyclovir. This is likely primarily due to the different pH of the donor solutions (i.e. 6.5 in this study and 7.4 in the previous study). In this study, the P_{app} of metoprolol, a weakly basic compound, was only approximately half of the P_{app} value measured in the previous study (5.98 ± 0.52 *vs* $10.0 \pm 0.3 \times 10^{-6}$ cm/s). According to the theory of dissociation, for weakly basic compounds a higher proportion of molecules is in their unionized form at pH 7.4 as compared to pH 6.5. The unionized proportion of a compound contributes to permeation to a higher degree. To confirm that the observed difference in metoprolol's P_{app} was due to the different pH, metoprolol's P_{app} was also determined at pH 7.4 using the Permeapad® 96-well plate. Figure 6 compares metoprolol's P_{app} values at pH 6.5 and 7.4 and confirms that metoprolol's P_{app} is increased when using donor solutions at higher pH. At the same donor pH value of 7.4, metoprolol's P_{app} determined in this study ($12.4 \pm 0.37 \times 10^{-6}$ cm/s) was comparable to the P_{app} value previously determined ($10.0 \pm 0.3 \times 10^{-6}$ cm/s). It is worth mentioning, however, that the increase in permeability with higher pH does not live up to theoretical expectations. According to the pH-partition theory the P_{app} values at pH 7.4 should be approximately 7.9 times higher than those at pH 6.5. The pH-dependence of metoprolol P_{app}, however, fits fairly well with that of intestinal loop segmental permeability differences reported by Dahan' s group (25). The interested reader is also referred to a previous study, where the pH-effect on Permeapad® permeability is discussed in detail and compared to alternative permeation screens (26). Another reason for the relatively low permeation of metoprolol may be the phospholipid composition of the Permeapad® barrier, which mainly consists of the neutral (zwitterionic) phosphatidylcholine (Lipoid S100). Polli' s group identified ion-pairing of metoprolol with negatively charged phospholipids as transport mechanism over PAMPA barriers (27). The presence of negatively charged phospholipids (phosphatidylserine) in the PAMPA barrier induced higher P_{app} values of metoprolol as compared to the zwitterionic phosphatidylcholine. To clarify whether an ion-pairing mechanism is involved in the transport of metoprolol across Permeapad®, further studies that include negatively charged phospholipids are needed. At the same time, this may help to explain, why metoprolol, which generally is regarded a borderline permeability marker, showed a lower permeability than acyclovir, norfloxacin and terbutaline.

The current study included compounds that have not been investigated in the Permeapad® model previously, namely antipyrine, carbamazepine, enalapril, lucifer yellow, naproxen, norfloxacin, sulpiride and terbutaline. These compounds were selected, because they are commonly used for validation of permeation models. In combination with the previously investigated compounds, the current set of model compounds not only reflects a wide range of physicochemical properties (Table I) but also different degrees of absorption (i.e. expressed as the fraction absorbed in humans; F_a; Table IV).

When plotting literature values of the F_a against the Permeapad® P_{app} values, a hyperbolic correlation is obtained (Fig. 7a). Similar hyperbolic correlations between F_a and P_{app} have been described for the PAMPA model (3,28), the PVPA model (6) and the Caco-2 model (29). For easy and visual comparison, Fig. 7b illustrates the correlation between F_a and literature Caco-2 P_{app} values (30–37) of the 12 model

Table IV The fraction absorbed in humans (F_a)[a], Permeapad® apparent permeability (P_{app}) measured in the Permeapad® 96-well plate, Permeapad® P_{app} measured with the in-house prepared barrier[c], literature Caco-2 P_{app} values and literature PAMPA P_{app} values

Compound no	Compound	F_a (%)[a]	Permeapad® P_{app} ± SD (10^{-6} cm/s)[b]	In-house prepared Permeapad® P_{app} ± SD (10^{-6} cm/s)[c]	Caco-2 P_{app} ± SD (10^{-6} cm/s)	PAMPA P_{app} (10^{-6} cm/s)[a] at pH 5.5 & 7.4	Reference for Caco-2 P_{app}
1	Acyclovir	21	6.44 ± 1.26	7.9 ± 1.3	0.25 ± 0.03	0.0 & 0.0	Yazdanian *et al.* (30)
2	Antipyrine	100	18.6 ± 1.10	–	33.1 ± 1.2	20.1 & 13.2	Yamashita *et al.* (31)
3	Caffeine	100	29.3 ± 2.51*	20.4 ± 3.2	30.8 ± 1.5	20.6 & 10.8	Yazdanian *et al.* (30)
–	Calcein	–	0.43 ± 0.04	1.2 ± 0.1	0.33 ± 0.21	–	Ghartey-Tagoe *et al.* (32)
4	Carbamazepine	100	18.6 ± 1.20	–	13.16 ± 3	12.0 & 11.3	Kogan *et al.* (33)
5	Enalapril	60	4.13 ± 0.21*	–	3.12 ± 0.1	3.4 & 0.1	Morrison *et al.* (34)
6	Hydrocortisone	91	12.3 ± 0.52	12.7 ± 1.5	14 ± 2.6	3.1 & 3.4	Yazdanian *et al.* (30)
–	Lucifer Yellow	0	2.98 ± 0.55	–	0.18 ± 0.035	0.0 & 0.0	Antonescu *et al.* (35)
7	Metoprolol	95	5.98 ± 0.52	10.0 ± 0.3	23.7 ± 1.3	1.2 & 3.5	Yazdanian *et al.* (30)
8	Nadolol	32	2.51 ± 0.40*	6.0 ± 0.6	3.88 ± 0.48	0.0 & 0.0	Yazdanian *et al.* (30)
9	Naproxen	98	29.1 ± 3.37	–	39.5 ± 0.3	22.9 & 10.6	Pade and Stavchansky (36)
10	Norfloxacin	35	6.57 ± 0.45	–	0.17 ± 0.03	0.5 & 0.9	Takenaka *et al.* (37)
11	Sulpiride	36	5.40 ± 0.94	–	0.17 ± 0.02	0.2 & 0.1	Takenaka *et al.* (37)
12	Terbutaline	68	6.39 ± 0.41	–	0.47 ± 0.08	0.0 & 0.1	Yazdanian *et al.* (30)

[a] Values for the fraction absorbed in humans and PAMPA P_{app} were taken from Zhu *et al.* (28). SDs for PAMPA P_{app} values were not reported by Zhu *et al.* (28).[b] Permeapad® P_{app} determined using the 96-well format is expressed as the mean of 6 replicates, unless marked with * then the P_{app} is expressed as the mean of 3–4 replicates. [c] In-house prepared Permeapad® P_{app} values determined at pH 7.4 were taken from Di Cagno *et al.* (7)

drugs used in this study. Here, the number of publications was kept to a minimum to avoid interlaboratory variations that often are experienced in the Caco-2 model. The hyperbolic correlation includes a steep slope region and a plateau region. Drugs in the steep slope region are considered poorly to moderately absorbed whereas drugs in the plateau region are considered well absorbed.

In the Caco-2 model (Fig. 7b), the plateau region contains drugs with P_{app} values larger than 10×10^{-6} cm/s (i.e. antipyrine, caffeine, carbamazepine, hydrocortisone, metoprolol and naproxen). Generally, Caco-2 P_{app} values larger than 10×10^{-6} cm/s are considered to indicate high absorption (38). Similar to the Caco-2 model, 5 out of 6 high absorption drugs had P_{app} values larger than 10×10^{-6} cm/s in the Permeapad® 96-well plate (Fig. 7a). However, metoprolol, which despite its irregular behaviour (formation of ion-pairs (27)) typically is used to indicate the class boundary between low and high absorption (39), can be found in the steep slope region with a P_{app} of $5.98 \pm 0.52 \times 10^{-6}$ cm/s. As discussed above, metoprolol's P_{app} was highly dependent on the pH of the donor solution (Fig. 6). When the pH of the donor solution was increased, metoprolol's P_{app} was larger than 10×10^{-6} cm/s. This indicates that the Permeapad® 96-well plate seems to be rather sensitive towards changes in pH. The pH in the gastrointestinal tract is variable not only in different regions but also among individuals (40). To take the physiological and individual differences in pH and the sensitivity of the Permeapad® model towards pH into account, the P_{app} of compounds with pKa values in the physiological range of the gastrointestinal tract should be tested at several pH values. Thereby, a better picture of the drug's absorption probability can be obtained.

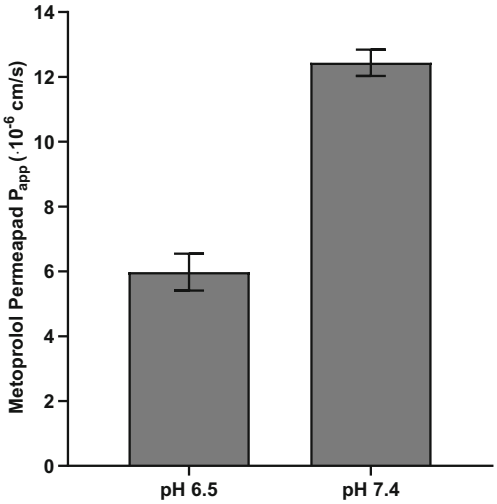

Fig. 6 The apparent permeability (Papp) of metoprolol at different pH of the donor solution. The acceptor medium was always PBS pH 7.4. Data is shown as the mean ± SD of 6 replicates.

The steep slope region contains drugs with P_{app} values of approximately 0.2 to 4×10^{-6} cm/s in the Caco-2 model (i.e. acyclovir, enalapril, nadolol, norfloxacin, sulpiride and terbutaline). In the Permeapad® 96-well plate, the P_{app} values of these drugs of the steep slope region are approximately 2.5 to 6.5×10^{-6} cm/s. Hence, the absolute P_{app} values within this region are slightly higher in the Permeapad® 96-well plate. When comparing to absolute Caco-2 or also PAMPA permeabilities (PAMPA is discussed in more detail below), it could appear that the Permeapad® may overestimate the permeability of these compounds. However, these compounds still have F_a = 21–68%. Hence it can be argued that the other *in vitro* models may underestimate the permeabilities of these compounds to a certain degree, e.g. terbutaline has a F_a of 68% and in the PAMPA and Caco-2 model this compound has virtually no permeation (See Table I).

Even though the permeabilities of the compounds in the steep slope region generally are higher, it is still possible to clearly distinguish high absorption compounds from low/moderate absorption compounds when using the Permeapad® 96 well-plate. In more detail, in the Permeapad® model, P_{app} values above 10×10^{-6} cm/s indicate high permeability (plateau region of Fig. 7a) and P_{app} values below 10×10^{-6} cm/s indicate low or moderate permeability (steep slope region of Fig. 7a). In many *in vitro* permeability assays the weak base metoprolol (F_a = 95%) is used to indicate the border between high and low/moderate permeability compounds. Due to the pH depended permeability and the possibility of ion-pair mediated transport as discussed above, we recommend the neutral compound hydrocortisone (F_a = 91%) to indicate the border between high and low/moderate permeability compounds in the Permeapad® assay instead. It has to be emphasized that moderate absorption compounds (F_a = 55–80%) cannot clearly be distinguished from low absorption compounds (F_a < 55%) in the Permeapad® model. For example, enalapril (F_a = 60%) had a lower P_{app} value than acyclovir (F_a = 21%) or norfloxacin (F_a = 35%). Also in the Caco-2 model, it is difficult to distinguish moderate and low absorption drugs. For example, terbutaline (F_a = 68%) had a lower P_{app} than nadolol (F_a = 32%). This 'blind spot' phenomenon has previously been recognized in literature (41). One likely explanation for the 'blind spot' phenomenon is the challenge to reflect physiological and inter-individual differences in *in vitro* assays.

The Permeapad® model and the Caco-2 model have a similar hyperbolic correlation to F_a as illustrated in Fig. 7. Taking this a step further, Fig. 8 attempts a direct correlation of the two models. Previously, a reasonable linear correlation between the in-house prepared Permeapad® and the Caco-2 model has been described (7). In this previous study, the coefficient of determination (R^2) was 0.75 with exclusion of theophylline. Theophylline was excluded due to the possibility of an active transport mechanism, which cannot be mimicked by the Permeapad® model. The extended data set of the current study confirms a reasonable correlation (R^2 = 0.70). It should be noted that the Caco-2 studies referenced here were carried out at pH 7.2–7.4 whereas this study was carried out at pH 6.5. The P_{app} of metoprolol was highly affected by pH. This is also reflected in the direct correlation. When replacing metoprolol's P_{app} at pH 6.5 with its P_{app} at pH 7.4, a better linear correlation (R^2 = 0.81) was found.

Even though a reasonable correlation between the Permeapad® model and the Caco-2 model was observed, a distinct functional difference between the two models exists. In contrast to the Caco-2 model, the Permeapad® model, like all non-cellular models, is inherently unable to mimic active transport mechanisms. Therefore, a set of 12 predominantly passively absorbed compounds was selected for the current study. To reveal the impact of alternative transport pathways, obviously cell-based or tissue-based permeation models must be employed where transport proteins are expressed, and tight junctions formed.

The restriction to passive transport pathways is a feature common to all non-cellular permeation models of which the PAMPA model was firstly described (3) and is widely used. In an attempt to compare the performance of the two artificial permeation models, P_{app} values obtained by using the Permeapad® 96-well plate with gradient pH (i.e. pH 6.5 in the donor and pH 7.4 in the acceptor) were plotted against published P_{app} values obtained by using a PAMPA model (see Fig. 9). Here, published PAMPA P_{app} values from Zhu *et al.* (28) were used where the pH was either 5.5 (Fig. 9a) or 7.4 (Fig. 9b). Figure 9a shows a good linear correlation between the Permeapad® and the PAMPA model at a pH of 5.5 (R^2 = 0.89). At a pH of 7.4, the correlation was reasonable (R^2 = 0.70) and comparable to the correlation with the Caco-2

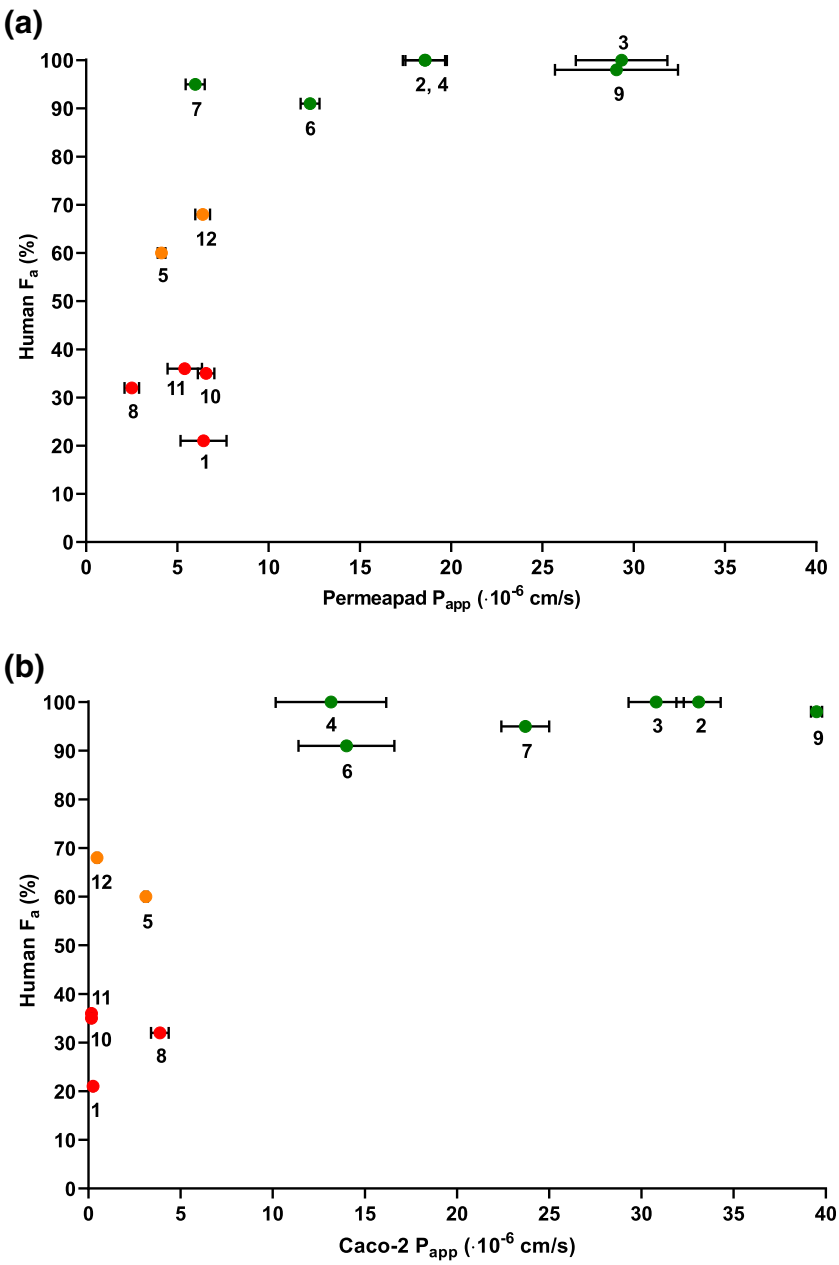

Fig. 7 The fraction absorbed in humans (F_a) plotted against the apparent permeability (P_{app}) of the model compounds determined in (**a**) the Permeapad® 96-well plate or (**b**) the Caco-2 model. Caco-2 P_{app} values were taken from literature (see Table IV for references). Red, orange and green circles indicate poorly absorbed (F_a < 55%), moderately absorbed (F_a = 55–80%) and well absorbed (F_a > 80%) compounds, respectively. Numbers indicate the model compounds: 1) acyclovir, 2) antipyrine, 3) caffeine, 4) carbamazepine, 5) enalapril, 6) hydrocortisone, 7) metoprolol, 8) nadolol, 9) naproxen, 10) norfloxacin, 11) sulpiride and 12) terbutaline.

model (see Fig. 9b). This underlines the impact of pH on permeation of compounds with pKa values in the physiological range. It should be mentioned that the PAMPA values from Zhu *et al.* (28) were reported without SD. Untypically, Zhu and co-workers used a PAMPA model consisting of a hydrophilic filter soaked in a 1% egg-lecithin solution in n-dodecane (28). Hydrophobic filter material is more commonly used (2). Even though no SDs are reported in this study and hydrophilic filter material was used, the study by Zhu and co-workers was selected for comparison because it contains all compounds investigated here. Thereby, inter-study variations due to differences in filter material and lipid composition were avoided.

The set-up employed by Zhu appears to underestimate the permeability of hydrocortisone, while the permeability of hydrocortisone indicated by Permeapad® fits well with that of Caco-2 permeability. This could be due to the presence of organic solvent, believed to form the core of PAMPA-barriers. Hydrocortisone's permeability through the organic solvent-based barrier may be different than its permeability through the bilayers in the Permeapad® barrier and the Caco-2 monolayer, which are closer to the physiological scenario. Furthermore, the low, yet significant permeability of Lucifer Yellow, which generally is regarded as a paracellular marker, may indicate that Permeapad®, in contrast to PAMPA, may to some extent

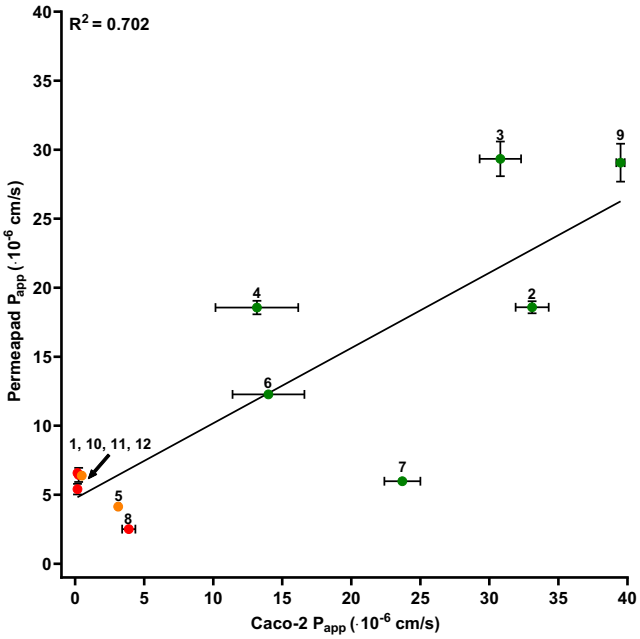

Fig. 8 The apparent permeability (P_{app}) determined in the Permeapad® 96-well plate plotted against literature Caco-2 P_{app} values (see Table IV for references). Red, orange and green circles indicate poorly absorbed (F_a < 55%), moderately absorbed (F_a = 55–80%) and well absorbed (F_a > 80%) compounds, respectively. Numbers indicate the model compounds: 1) acyclovir, 2) antipyrine, 3) caffeine, 4) carbamazepine, 5) enalapril, 6) hydrocortisone, 7) metoprolol, 8) nadolol, 9) naproxen, 10) norfloxacin, 11) sulpiride and 12) terbutaline.

allow permeation along water-channels across the barrier. This observation is further supported by the relatively high permeability of the marker calcein and those of drug compounds, which are believed to be transported (partially) via the paracellular pathway *in vivo*, like acyclovir, nadolol, sulpiride and terbutaline. This hypothesis certainly needs further experimental clarification by e.g. fluorescence microscopic studies.

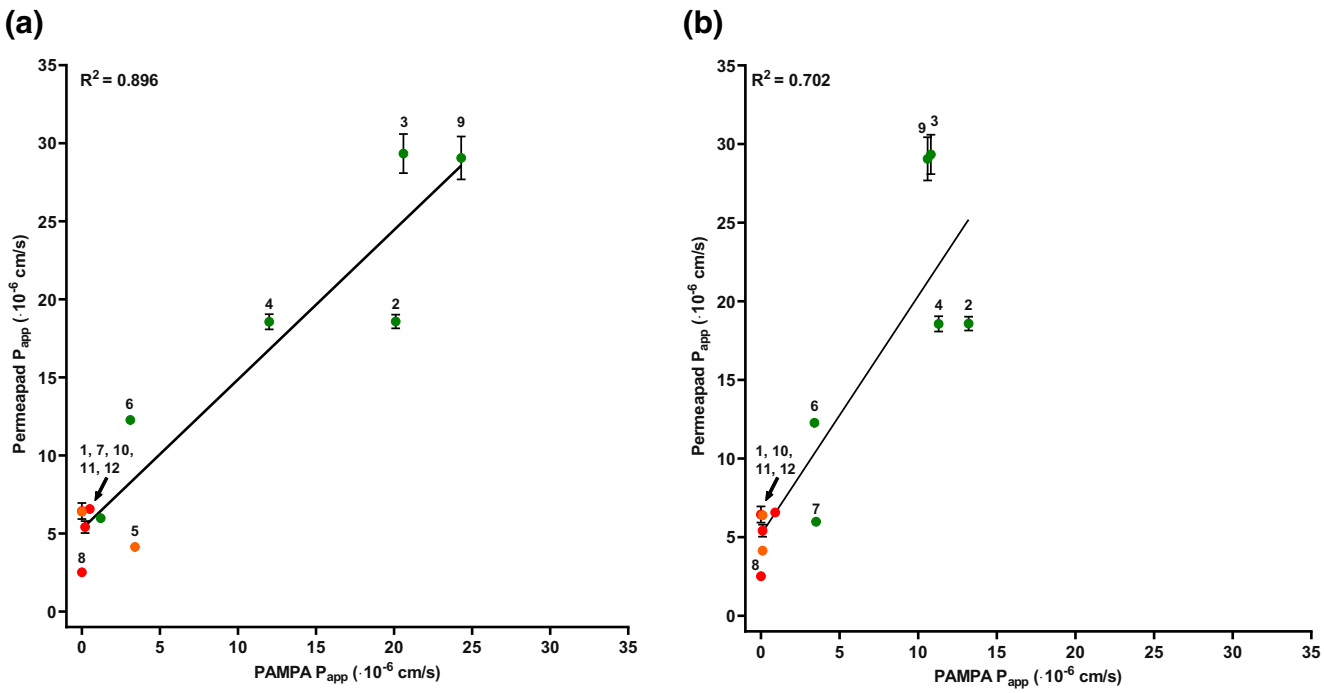

Fig. 9 The apparent permeability (P_{app}) determined in the Permeapad® 96-well plate using gradient pH (i.e. pH 6.5 in the donor and pH 7.4 in the acceptor) plotted against literature PAMPA P_{app} values from Zhu *et al.* (28) determined at (**a**) pH 5.5 and (**b**) pH 7.4. Red, orange and green circles indicate poorly absorbed (F_a < 55%), moderately absorbed (F_a = 55–80%) and well absorbed (F_a > 80%) compounds, respectively. Numbers indicate the model compounds: 1) acyclovir, 2) antipyrine, 3) caffeine, 4) carbamazepine, 5) enalapril, 6) hydrocortisone, 7) metoprolol, 8) nadolol, 9) naproxen, 10) norfloxacin, 11) sulpiride and 12) terbutaline.

CONCLUSION

This study demonstrates that the Permeapad® 96-well plate is a promising addition to the drug permeability profiling toolbox. The Permeapad® 96-well plate allows fast and reproducible permeation experiments. The experimental permeability values obtained allowed clearly to distinguish high- from moderate−/low-absorption drugs and yielded a hyperbolic correlation with human F_a, which is typical for *in vitro* permeability data. According to this study, P_{app} values above 10×10^{-6} cm/s indicate high permeability in the Permeapad® permeation assay. The neutral molecule hydrocortisone, instead of the weak base metoprolol, is regarded suitable to indicate the class boundary between high and moderate-to-low absorption. Permeapad®, in contrast to PAMPA, appears to allow the minor passage of drug compounds with an established paracellular absorption pathway, which may serve as a first indication for the presence of water-filled pores across Permeapad®. This observation deserves further investigation. Although the Permeapad® Plate comprises an industrially produced version of the Permeapad® barrier, the permeability values are fully comparable with those, obtained with the Permeapad® barrier made in-house and employed with a Franz cell set-up. Compared to the latter, the microtiter plate format substantially increases the throughput and renders the Permeapad® 96-well plate a veritable high-throughput tool. The permeability values obtained with the Permeapad® 96-well plate correlated reasonably well with published permeability data obtained via the Caco-2 model and very well with those obtained via a PAMPA model. The microscopic images of the Permeapad® barrier upon swelling revealed large phospholipid vesicles and myelin-structures.

Acknowledgements and Disclosures. The authors would like to acknowledge InnoMe GmbH, Espelkamp, Germany for providing prototype Permeapad® plates and financial support towards a PhD-position for ACJ. This article is partly based upon work carried out under COST Action 16205 UNGAP, supported by COST (European Cooperation in Science and Technology) as well as Nordic POP (Patient Oriented Products), a Nordic University Hub funded by NordForsk (Project number: 85352). Furthermore, the authors would like to acknowledge Tina Christiansen for her excellent support with UHPLC-UV analyses.

DISCLAIMER

The sponsor has not taken any influence on study design, data interpretation or writing of the current manuscript.

REFERENCES

1. Sugano K, Kansy M, Artursson P, Avdeef A, Bendels S, Di L, et al. Coexistence of passive and carrier-mediated processes in drug transport. Nat Rev Drug Discov. 2010;9:597–614.
2. Berben P, Bauer-Brandl A, Brandl M, Faller B, Flaten GE, Jacobsen A-C, et al. Drug permeability profiling using cell-free permeation tools: overview and applications. Eur J Pharm Sci. 2018;119:219–33.
3. Kansy M, Senner F, Gubernator K. Physicochemical high throughput screening: parallel artificial membrane permeation assay in the description of passive absorption processes. J Med Chem American Chemical Society. 1998;41:1007–10.
4. Teksin ZS, Seo PR, Polli JE. Comparison of drug Permeabilities and BCS classification: three lipid-component PAMPA system method versus Caco-2 monolayers. AAPS J. 2010;12:238–41.
5. Avdeef A, Artursson P, Neuhoff S, Lazorova L, Gråsjö J, Tavelin S. Caco-2 permeability of weakly basic drugs predicted with the double-sink PAMPA pKaflux method. Eur J Pharm Sci. 2005;24:333–49.
6. Flaten GE, Dhanikula AB, Luthman K, Brandl M. Drug permeability across a phospholipid vesicle based barrier: a novel approach for studying passive diffusion. Eur J Pharm Sci. 2006;27:80–90.
7. di Cagno M, Bibi HA, Bauer-Brandl A. New biomimetic barrier Permeapad™ for efficient investigation of passive permeability of drugs. Eur J Pharm Sci. 2015;73:29–34.
8. Lasic DD. Structure of amphiphilic aggregates. In: D.D. Lasic, editor. Liposomes from Phys to Appl. Elsevier Amsterdam; 1993. p. 43–62.
9. Volkova T V, Terekhova I V, Silyukov OI, Proshin AN, Bauer-Brandl A, Perlovich GL. Towards the rational design of novel drugs based on solubility, partitioning/distribution, biomimetic permeability and biological activity exemplified by 1,2,4-thiadiazole derivatives. Medchemcomm. The Royal Society of Chemistry; 2017;8:162–175.
10. Bibi HA, di Cagno M, Holm R, Bauer-Brandl A. Permeapad™ for investigation of passive drug permeability: the effect of surfactants, co-solvents and simulated intestinal fluids (FaSSIF and FeSSIF). Int J Pharm. 2015;493:192–7.
11. Volkova TV, Domanina EN, Kumeev RS, Proshin AN, Terekhova IV. The effect of different polymers on the solubility, permeability and distribution of poor soluble 1,2,4-thiadiazole derivative. J Mol Liq. 2018;269:492–500.
12. Bibi HA, Holm R, Bauer-Brandl A. Simultaneous lipolysis/permeation in vitro model, for the estimation of bioavailability of lipid based drug delivery systems. Eur J Pharm Biopharm. 2017;117:300–7.
13. Fong SYK, Martins SM, Brandl M, Bauer-Brandl A. Solid phospholipid dispersions for Oral delivery of poorly soluble drugs: investigation into Celecoxib incorporation and solubility-in vitro permeability enhancement. J Pharm Sci. 2016;105:1113–23.
14. Jacobsen A-C, Elvang PA, Bauer-Brandl A, Brandl M. A dynamic in vitro permeation study on solid mono- and diacyl-phospholipid dispersions of celecoxib. Eur J Pharm Sci. 2019;127:199–207.
15. Wu IY, Bala S, Škalko-Basnet N, di Cagno MP. Interpreting non-linear drug diffusion data: Utilizing Korsmeyer-Peppas model to study drug release from liposomes. Eur J Pharm Sci 2019;138:105026.
16. Agafonov M, Volkova T, Kumeev R, Chibunova E, Terekhova I. Impact of pluronic F127 on aqueous solubility and membrane permeability of antirheumatic compounds of different structure and polarity. J Mol Liq. 2019;274:770–7.
17. Volkova T, Kumeev R, Kochkina N, Terekhova I. Impact of Pluronics of different structure on pharmacologically relevant

properties of sulfasalazine and methotrexate. J Mol Liq. 2019;289: 111076.
18. Hermanson GT. Chapter 10 - fluorescent probes. In: Hermanson GTBT-BT (third E, editor. Boston: Academic Press; 2013. p. 395–463.
19. Brandl M, Tardi C, Drechsler M, Bachmann D, Reszka R, Bauer KH, et al. Three-dimensional liposome networks: freeze fracture electron microscopical evaluation of their structure and in vitro analysis of release of hydrophilic markers. Adv Drug Deliv Rev. 1997;24:161–4.
20. Brandl M. Vesicular phospholipid gels: a technology platform. J Liposome Res Taylor & Francis. 2007;17:15–26.
21. Sugano K. 5.19 - Artificial Membrane Technologies to Assess Transfer and Permeation of Drugs in Drug Discovery. In: Taylor JB, Triggle DJBT-CMCII, editors. Oxford: Elsevier; 2007. p. 453–487.
22. Flaten GE, Bunjes H, Luthman K, Brandl M. Drug permeability across a phospholipid vesicle-based barrier: 2. Characterization of barrier structure, storage stability and stability towards pH changes. Eur J Pharm Sci. 2006;28:336–43.
23. Karlsson J, Artursson P. A method for the determination of cellular permeability coefficients and aqueous boundary layer thickness in monolayers of intestinal epithelial (Caco-2) cells grown in permeable filter chambers. Int J Pharm. 1991;71:55–64.
24. Nielsen PE, Avdeef A. PAMPA—a drug absorption in vitro model: 8. Apparent filter porosity and the unstirred water layer. Eur J Pharm Sci. 2004;22:33–41.
25. Wolk O, Markovic M, Porat D, Fine-Shamir N, Zur M, Beig A, Dahan A. Segmental-dependent intestinal drug permeability: development and model validation of In silico predictions Guided by In Vivo permeability values. J Pharm Sci Elsevier; 2019;108:316–325.
26. Bibi HA, Holm R, Bauer-Brandl A. Use of Permeapad® for prediction of buccal absorption: a comparison to in vitro, ex vivo and in vivo method. Eur J Pharm Sci. 2016;93:399–404.
27. Teksin ZS, Hom K, Balakrishnan A, Polli JE. Ion pair-mediated transport of metoprolol across a three lipid-component PAMPA system. J Control Release. 2006;116:50–7.
28. Zhu C, Jiang L, Chen T-M, Hwang K-K. A comparative study of artificial membrane permeability assay for high throughput profiling of drug absorption potential. Eur J Med Chem. 2002;37:399–407.
29. Artursson P, Karlsson J. Correlation between oral drug absorption in humans and apparent drug permeability coefficients in human intestinal epithelial (Caco-2) cells. Biochem Biophys Res Commun. 1991;175:880–5.
30. Yazdanian M, Glynn SL, Wright JL, Hawi A. Correlating partitioning and Caco-2 cell permeability of structurally diverse small molecular weight compounds. Pharm Res. 1998;15:1490–4.
31. Yamashita S, Furubayashi T, Kataoka M, Sakane T, Sezaki H, Tokuda H. Optimized conditions for prediction of intestinal drug permeability using Caco-2 cells. Eur J Pharm Sci. 2000;10:195–204.
32. Ghartey-Tagoe EB, Morgan JS, Neish AS, Prausnitz MR. Increased permeability of intestinal epithelial monolayers mediated by electroporation. J Control Release. 2005;103:177–90.
33. Kogan A, Kesselman E, Danino D, Aserin A, Garti N. Viability and permeability across Caco-2 cells of CBZ solubilized in fully dilutable microemulsions. Colloids Surfaces B Biointerfaces. 2008;66:1–12.
34. Morrison RA, Chong S, Marino AM, Wasserman MA, Timmins P, Moore VA, et al. Suitability of Enalapril as a probe of the dipeptide transporter system: InVitro and in vivo studies. Pharm Res. 1996;13:1078–82.
35. Antonescu IE, Rasmussen KF, Neuhoff S, Fretté X, Karlgren M, Bergström CAS, et al. The permeation of Acamprosate is predominantly caused by Paracellular diffusion across Caco-2 cell monolayers: a Paracellular modeling approach. Mol Pharm. American Chemical Society. 2019;16:4636–50.
36. Pade V, Stavchansky S. Link between drug absorption solubility and permeability measurements in Caco-2 cells. J Pharm Sci Elsevier. 1998;87:1604–7.
37. Takenaka T, Harada N, Kuze J, Chiba M, Iwao T, Matsunaga T. Application of a human intestinal epithelial cell monolayer to the prediction of Oral drug absorption in humans as a superior alternative to the Caco-2 cell monolayer. J Pharm Sci. 2016;105:915–24.
38. Yee S. In vitro permeability across Caco-2 cells (colonic) can predict in vivo (small intestinal) absorption in man—fact or myth. Pharm Res. 1997;14:763–6.
39. Zur M, Gasparini M, Wolk O, Amidon GL, Dahan A. The low/high BCS permeability class boundary: physicochemical comparison of Metoprolol and labetalol. Mol Pharm American Chemical Society. 2014;11:1707–14.
40. Vertzoni M, Augustijns P, Grimm M, Koziolek M, Lemmens G, Parrott N, et al. Impact of regional differences along the gastrointestinal tract of healthy adults on oral drug absorption: an UNGAP review. Eur J Pharm Sci. 2019;134:153–75.
41. Lüpfert C, Reichel A. Development and application of physiologically based pharmacokinetic-modeling tools to support drug discovery. Chem Biodivers. John Wiley & Sons, Ltd; 2005;2:1462–86.